LEAD ACID BATTERY MODELING FOR PHOTOVOLTIAC APPLICATIONS

Rami HADDAD Adel EL SHAHAT Youakim KALAANI
Department of Electrical Engineering, Georgia Southern University, Statesboro, GA, USA
rhaddad@georgiasouthern.edu, aahmed@georgiasouthern.edu,

Abstract: *Lead-Acid batteries continue to be the preferred choice for backup energy storage systems. However, the inherent variability in the manufacturing and component design processes affect the performance of the manufactured battery. Therefore, the developed Lead-Acid battery models are not very flexible to model this type of variability. In this paper, a new and flexible modeling of a Lead-Acid battery is presented. Using curve fitting techniques, the model parameters were derived as a function of the battery's state of charge based on a modified Thevenin equivalent model. In addition, the charge and discharge characteristics of the derived model were investigated and validated using a real NP4-12 YUASA battery manufacturer's data sheet to match performance at different capacity rates. Furthermore, an artificial neural network based learning system with back-propagation technique was used for estimating the model parameters using MATLAB software. The proposed neural model had the ability to predict values and interpolate between the learning curves data at various characteristics without the need of training. Finally, a closed-form analytical model that connects between inputs and outputs for neural networks was presented. It was validated by comparing the target and output and resulted in excellent regression factors.*

Key words: *Lead-Acid Battery, Storage, Model, Neural Network, and Estimation.*

1. Introduction.

Advances in energy storage technologies are spearheaded the by significant improvements in the dynamic performance of storage batteries making them cost-effective and more efficient. Lead-Acid batteries continue to be the main energy storage unit (ESU) for a wide range of applications such as hybrid electric vehicles (HEV) and photovoltaic (PV) systems. Depending on the application, ESU has the ability to either receive or deliver power via a DC/AC inverter. Currently, there are several types of batteries classified according to cost, size, and service lifetime. Batteries with good energy density suffer typically from poor power density and must be supplemented by supercapacitors to provide for short power peaks in power systems [36].

In high power applications, there are two main energy storage technologies utilized, namely the Nickel-metal hydride NiMH and the lithium-ion (Li-Ion) [32]. The NiMH battery is a successor to the NiCd which has inherent issues such as the negative temperature coefficient, thermal runaway, and the toxicity of its chemicals to the environment. The introduction of NiMH technology allowed for 40% increase in specific energy capacity but at the expenses of lower charge-discharge cycles rate (approximately 500 at 1hr charge-1hr discharge rate) [33]. Another relatively new type of battery which has good electrical properties for high power applications is the Lithium-ion (Li-ion) battery. Li-ion battery has higher power density and can charge and discharge at a faster rate (approximately 1200 at 1hr charge - 1hr discharge rate). The cell potential is also considered high with an open circuit voltage of typically 4.15V per cell. However, the voltage level of Li-ion batteries must be continuously monitored since overcharging can lead to a thermal runaway condition which can destroy the battery [33]. Fig. 1 presents the Ragone chart to compare the performance of various types of energy-storing devices.

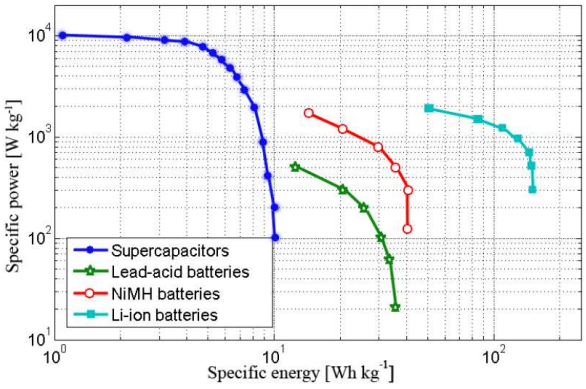

Fig. 1- Ragone chart comparing power density vs. energy density for various energy-storing devices [31]

A battery stores and delivers electrical power through electrochemical processes resulting in internal heat losses. The maximum capacity of a battery is closely related to the state of health (SoH) of the battery. A battery is considered "dead" when its capacity is down to 80% of the maximum capacity. In addition, the

efficiency of a battery is affected by heat losses in its equivalent internal resistor and can significantly shorten the life of the battery. The aging process of a NiMH battery is related to operation, temperature, charging/discharging cycles, and depth of discharge (DOD) of each cycle. NiMH battery has a high tendency to be overcharged which negatively impact its life cycle [34]. On the other hand, Lead-Acid batteries charging process can be easily controlled to avoid overcharging. In addition, the Li-ion battery has a more complex aging process that is less sensitive to overcharging but very sensitive to low temperatures [33]. A study of various energy storage technologies with a qualitative comparison was provided in [37]. The designing and sizing of an integrated solar and wind based hybrid for HEV charging system was presented in [42]. This system is comprised of a battery stack and super capacitors that can be automatically controlled using computer and interfacing circuits.

The Lead-Acid technology reached the maturity stage thus it has been used in a various engineering applications [4,5]. Using the state of charge (SOC) for modeling the Lead-Acid battery has been the key to improve its dynamic performance [12,13]. Several modeling techniques have been proposed using a neural network based learning system [14] and open circuit voltage (OCV) as a parameter to predict the SOC of the battery [15]. However, SOC estimation is particularly difficult due to considerable side reactions and losses that incur during the charging process. An equivalent-circuit model [16] is developed to estimate the battery SOC taking into consideration these effects.

2. Lead-Acid Battery Model

The basic battery model presented in [17] consisted of a simple resistor connected in series with an ideal voltage source. A more complex model however, is needed to capture the dynamic performance of Lead-Acid batteries [18, 19]. An enhanced dynamic model is shown in Fig. 2 where ohmic voltage drop and overvoltage effects are identified together and polarization resistance is described by a single equivalent resistor for each operating mode [20].

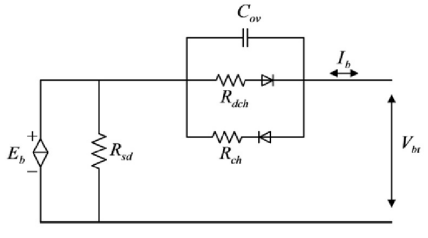

Fig. 2- Dynamic Model of a Lead-Acid Battery

As shown in Fig 2, the electric current, denoted by I_b flows through R_{ch} during charging and through R_{dch} during discharging. The self-discharge losses in the battery are modeled by R_{sd}. The terminal voltages of the battery are derived as:

$$V_{\text{bt\_chargin g}} = E_b + I_b R_{ch}\left(1 - e^{\frac{-t}{R_{ch}C_{ov}}}\right) \quad (1)$$

$$V_{\text{bt\_dischar ging}} = E_b - I_b R_{dch}\left(1 - e^{\frac{-t}{Rd_{ch}C_{ov}}}\right) \quad (2)$$

The overvoltage capacitance C_{ov} is estimated to be 40 F [20]. The dynamic characteristics of the battery depend on the battery SOC, the charge/discharge rate, and the electrolyte temperature. Based on the Yuasa (NP4-12) battery manufacturer's datasheet, the relationship between the battery open circuit voltage and remaining battery capacity is approximately linear [22] as depicted in Fig 3. Using the linear approximation technique, a function between E_b and SOC is given by:

$$E_b = 0.01375\,SOC + 11.5 \quad (3)$$

The values of R_{sd} are plotted versus the SOC as displayed in Fig 4. Using curve-fitting, a quadratic polynomial function for R_{sd} in kΩ as a function of the battery SOC is derived as:

$$R_{sd} = -0.039\,SOC^2 + 4.27\,SOC - 19.23 \quad (4)$$

Furthermore, the resistance R_{dch} is divided into two components [20]:

$$R_{dch} = R_{bdi} + R_{bd} \quad (5)$$

where

$$R_{bdi} = 1.01e^{-2.21 I_b} + 0.24e^{-0.06 I_b} \quad (6)$$

and

$$R_{bd} = 2.926\,e^{-0.042\,SOC} \quad (7)$$

During charging, R_{ch} can be divided into two components [20]:

$$R_{ch} = R_{bci} + R_{bc} \quad (8)$$

where R_{bci} is estimated to be 5 Ω, and

$$R_{bc} = 9.32 * 10^{-5} SOC^2 + 0.01 SOC + 0.028 \quad (9)$$

This proposed battery model is simulated as shown in Fig 3 at discharge rate of 0.1 CA. Terminal voltage V_{bt} is compared with the discharge characteristics given in the manufacturer's data sheet of the 12 V, 4 Ah *Yuasa batteries* [22]. Dotted line (---) represented the simulated discharge rate while the solid line (–)

represented the corresponding discharge rate from the manufacturer's data sheet. The comparison indicates a close match between the battery's actual and the modeled discharge rates.

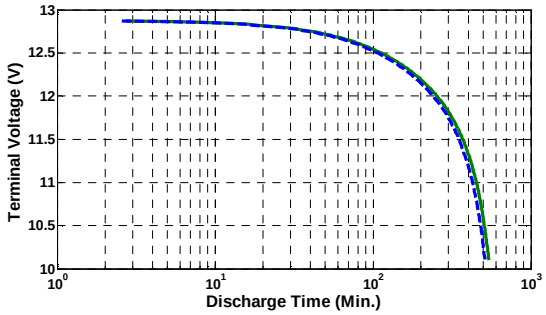

Fig. 3- Validation Results of the Battery Model at 0.1 CA

In addition, the battery model was simulated and validated for several discharge rates (0.5, 0.1, 0.2, 0.4, 0.6, 1, 2, and 3 CA). Again, terminal voltage V_{bt} is obtained in each case and compared with the discharge characteristics given in the manufacturer's data sheet as shown in Fig. 4. The validation results are displayed in Fig. 5. These comparisons also indicates close match between the actual and modeled discharge rates.

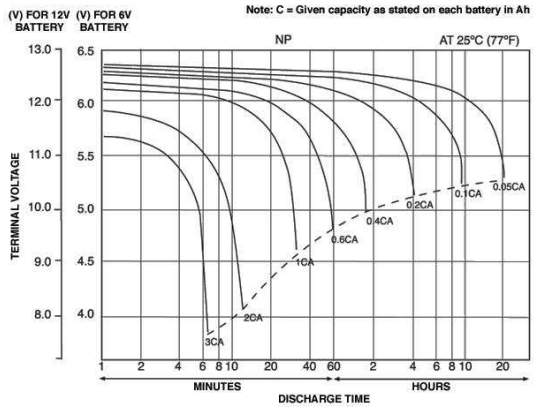

Fig. 4- Yuasa NP4-12 Discharge Characteristics Curves

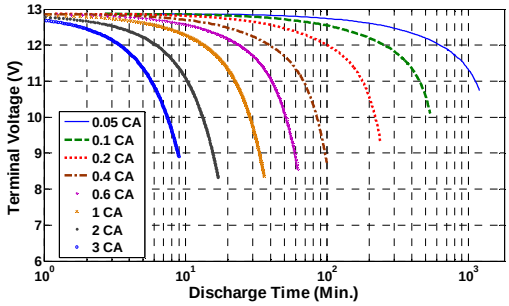

Fig. 5- Validation Results of the Battery Model at Various Discharge Rates

3. Neural Network Modeling

Artificial neural network (ANN) with back-propagation techniques [24,25] was used to implement charging and discharging models taking advantage of the ANN interpolation ability between points and curves for characteristics estimation. The closed-form algebraic equations representing the charging and discharging models were derived to be used without the need to retrain the neural network. The developed models have adequate number of layers and neurons with excellent regression constant as discussed below.

A. ANN Charging Model

For this model, the neural network inputs are Time, SOC, C (capacity rate) ranges and the outputs are $V_{bt\_charging}$, E_b, I_b, R_{sd} and R_{ch}. The model consists of a hidden layer with log-sig function and 7 neurons and a second layer with pure-line function and 5 neurons as shown in Fig 6.

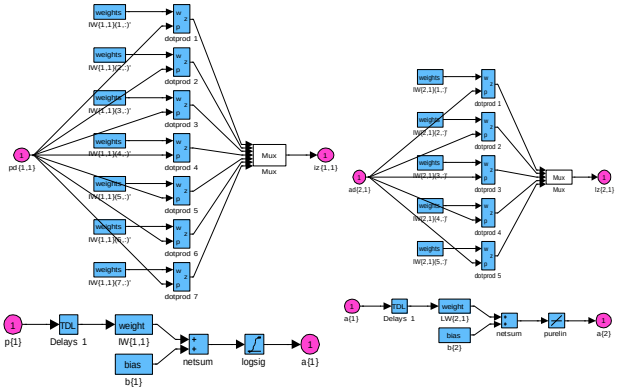

Fig. 6- 1st ANN Model with layers, neurons, weights, and structures

The training data was well depicted in the following 3D figures for all inputs (Fig. 7 – Fig. 9) and targets outputs (Fig 10) and regression (Fig 11).

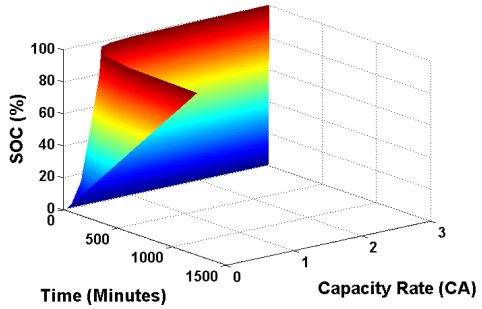

Fig. 7- 3D relation for SOC, CA with time for Charging Model

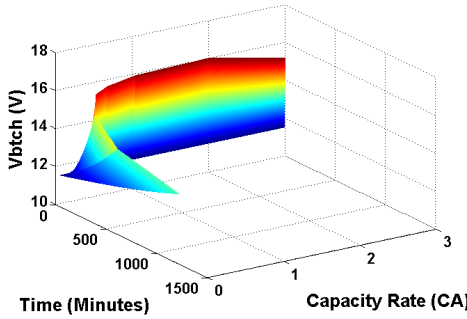

Fig. 8- 3D relation for V_{btch}, CA with time for Charging Model

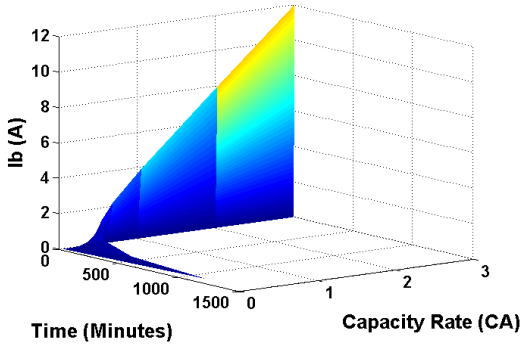

Fig. 9- 3D relation for I_b, CA with time for Charging Model

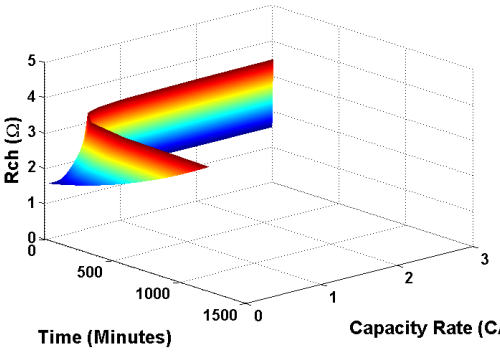

Fig. 10- 3-D relation for R_{ch}, CA with time for Charging Model

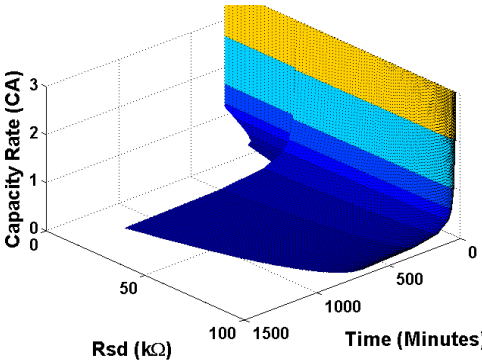

Fig. 11- 3-D relation for R_{sd}, CA with time for Charging Model

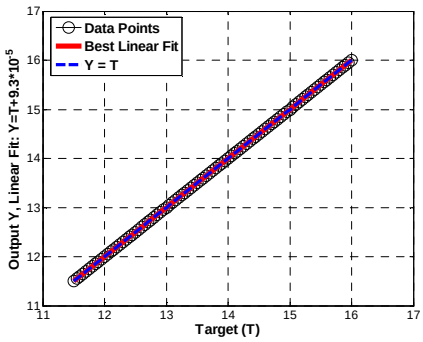

Fig. 12- Output VS Target for Charging Model

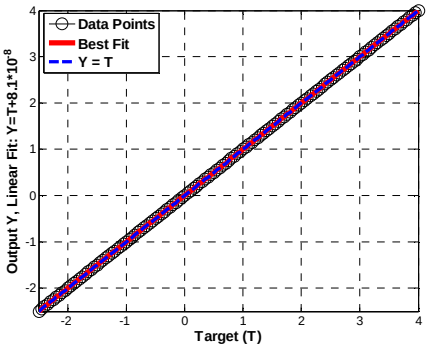

Fig. 13- Regression for Charging Model

The model mathematical formulation is presented in the following set of algebraic equations.

Normalized inputs (subscript *n* denotes normalized variable) for the ANN model

$$Time_n = 42.0849 * 10^{-4} Time - 0.579456 \quad (10)$$

$$SOC_n = 344.58 * 10^{-4} SOC - 1.7229 \quad (11)$$

$$CA_n = 1.0111 CA - 0.929 \quad (12)$$

Normalized outputs:

$$F_1 = \frac{1}{1 + e^{2*10^{-4} Time_n - 0.1051 SOC_n - 0.0527 CA_n - 1.5095}} \quad (13)$$

$$F_2 = \frac{1}{1 + e^{-0.1698 Time_n - 0.1299 SOC_n + 1.0518 CA_n + 1.5892}} \quad (14)$$

$$F_3 = \frac{1}{1 + e^{10^{-4} Time_n - 0.175 SOC_n - 0.0131 CA_n + 1.3759}} \quad (15)$$

$$F_4 = \frac{1}{1 + e^{10^{-4} Time_n + 0.0996 SOC_n - 0.0016 CA_n + 1.4836}} \quad (16)$$

$$F_5 = \frac{1}{1 + e^{-6*10^{-4} Time_n + 0.1366 SOC_n - 0.1024 CA_n - 1.3882}} \quad (17)$$

$$F_6 = \frac{1}{1 + e^{0.2581 Time_n - 0.0468 SOC_n + 0.7242 CA_n - 0.1513}} \quad (18)$$

$$F_7 = \frac{1}{1+e^{-0.0967\,Time_n+0.1745\,SOC_n+0.4317\,CA_n-1.6266}} \quad (19)$$

$$V_{btch_n} = -468.2F_1 - 46.7F_2 - 777.4F_3 - 175.7F_4 - 1170.1F_5 - 52.1F_6 - 143.3F_7 + 1665 \quad (20)$$

$$E_{b_n} = 1.6F_1 - 0.045F_2 - 12.3F_3 - 39.5F_4 - 1.7F_5 - 0.037F_6 + 0.049F_7 + 4.9 \quad (21)$$

$$I_{b_n} = -304.3F_1 + 1.3F_2 + 135.1F_3 - 380.6F_4 + 201.9F_5 + 1.2F_6 - 0.9F_7 + 130.6 \quad (22)$$

$$R_{sd_n} = 18.5F_1 + 0.6F_2 - 404.7F_3 - 847.5F_4 + 60.1F_5 + 0.5F_6 - 1.6F_7 + 177.1 \quad (23)$$

$$R_{ch_n} = -0.8F_1 - 0.1F_2 + 66.3F_3 + 71F_4 - 9.7F_5 - 0.1F_6 + 0.3F_7 - 18.4 \quad (24)$$

Un-normalized outputs

$$V_{btch} = 1.1591V_{btch_n} + 13.0038 \quad (25)$$

$$E_b = 0.399E_{b_n} + 12.1875 \quad (26)$$

$$I_b = 2.5233I_{b_n} + 1.8375 \quad (27)$$

$$R_{sd} = 31.269R_{sd_n} + 63.945 \quad (28)$$

$$R_{ch} = 0.5651R_{ch_n} + 2.3394 \quad (29)$$

B. ANN Discharging Model

Similarly for this model, the inputs are Time, SOC, C (capacity rate) ranges and the outputs are $V_{bt\_discharging}$, E_b, I_b, R_{sd} and R_{dch}. The model consists of a hidden layer with log-sig function and 10 neurons and a second layer with pure-line function and 5 neurons as displayed in Fig 12.

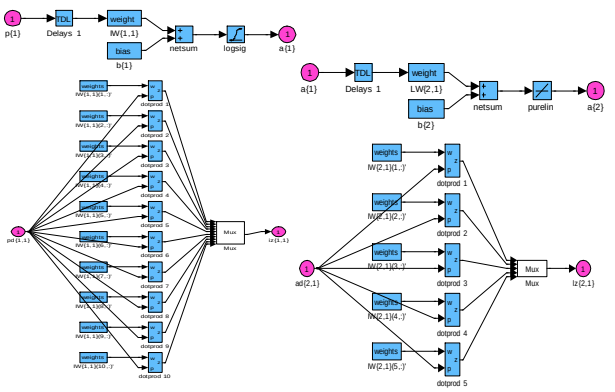

Fig. 14- 2nd ANN Model with its layers, neurons, weights, and structures

Again, the training data was well depicted in the following 3D figures for all inputs (Fig. 13-Fig. 15) and targets outputs (Fig. 16) and regression (Fig. 17).

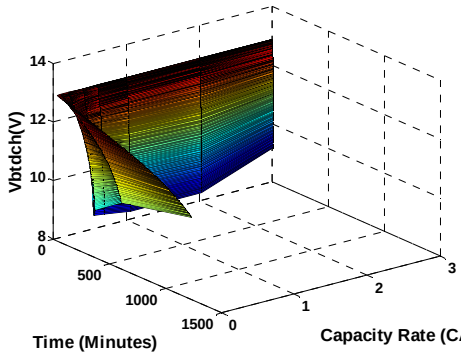

Fig. 15- 3D relation for V_{btdch}, CA with time for Discharging Model

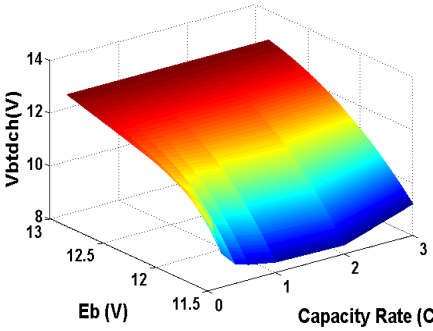

Fig. 16- 3D relation for V_{btdch}, E_b, with CA for Discharging Model

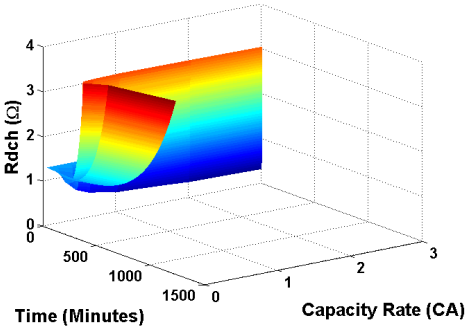

Fig. 17- 3D relation for R_{dch}, CA with time for Discharging Model

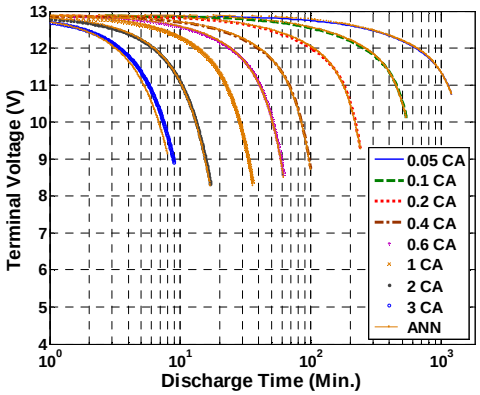

Fig. 18- Discharge voltage comparisons for all capacity ranges

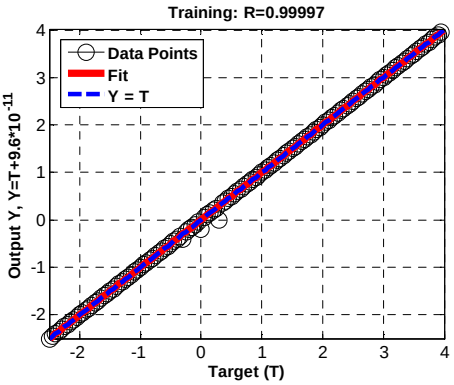

Fig. 19- Regression for Discharging Model

The model mathematical formulation is presented in the following set of algebraic equations:

$$F_1 = \frac{1}{1+e^{-143*10^{-4}Time_n - 0.7331SOC_n - 0.2524CA_n - 1.8208}} \quad (30)$$

$$F_2 = \frac{1}{1+e^{-0.1251Time_n + 1.685SOC_n - 0.2986CA_n - 3.9433}} \quad (31)$$

$$F_3 = \frac{1}{1+e^{-3.1084Time_n - 2.1596SOC_n + 0.3928CA_n + 2.0421}} \quad (32)$$

$$F_4 = \frac{1}{1+e^{-52*10^{-4}Time_n - 0.695SOC_n - 0.0176CA_n + 0.9002}} \quad (33)$$

$$F_5 = \frac{1}{1+e^{123*10^{-4}Time_n + 0.7279SOC_n + 0.233CA_n + 1.8247}} \quad (34)$$

$$F_6 = \frac{1}{1+e^{4.6783Time_n + 0.4329SOC_n - 1.4449CA_n + 3.2211}} \quad (35)$$

$$F_7 = \frac{1}{1+e^{59*10^{-4}Time_n + 0.7964SOC_n + 0.0233CA_n - 0.8382}} \quad (36)$$

$$F_8 = \frac{1}{1+e^{-3.2706Time_n - 2.2497SOC_n + 0.0288CA_n + 1.8566}} \quad (37)$$

$$F_9 = \frac{1}{1+e^{-0.3809Time_n - 0.8258SOC_n + 0.4331CA_n - 1.9203}} \quad (38)$$

$$F_{10} = \frac{1}{1+e^{69*10^{-4}Time_n + 0.6493SOC_n - 0.0605CA_n + 1.7393}} \quad (39)$$

$$V_{btdch_n} = -1085.2F_1 - 4.1F_2 - 2.5F_3 - 72.2F_4 - 1190.5F_5 - 0.9F_6 - 60.3F_7 + 2.4F_8 + 16.4F_9 + 107F_{10} + 1136.6 \quad (40)$$

$$E_{b_n} = 2.2F_1 + 0.2F_2 + 0.2F_3 + 16.3F_4 + 1.7F_5 + 9.8F_7 - 0.2F_8 - 0.2F_9 - 3.6F_{10} - 13.2 \quad (41)$$

$$I_{b_n} = -142.7F_1 - 1.9F_2 + 2F_3 - 39.1F_4 - 176.9F_5 - 0.2F_6 - 31.7F_7 - 1.9F_8 + 0.4F_9 + 37.4F_{10} + 176.8 \quad (42)$$

$$R_{sd_n} = -116.2F_1 + 0.2F_2 - 0.4F_3 - 107.4F_4 - 131.9F_5 + 0.1F_6 - 74.4F_7 + 0.4F_8 - 0.3F_9 - 23.8F_{10} + 205.9 \quad (43)$$

$$R_{dch_n} = -250.4F_1 + 58.8F_2 + 42F_3 + 1213.8F_4 - 238.2F_5 + 1.2F_6 + 961.9F_7 - 41.3F_8 + 4.5F_9 + 114.6F_{10} - 853.5 \quad (44)$$

Un-normalized outputs

$$V_{btdch} = 1.098V_{btch_n} + 11.5007 \quad (45)$$

$$E_b = 0.399E_{b_n} + 12.1875 \quad (46)$$

$$I_b = 2.5233I_{b_n} + 1.8375 \quad (47)$$

$$R_{sd} = 31.269R_{sd_n} + 63.945 \quad (48)$$

$$R_{dch} = 0.7085R_{ch_n} + 1.2383 \quad (49)$$

From these charging and discharging figures, it is evident that; the battery electromotive force is linearly proportional to battery capacity; however, with time the relationship becomes non-linear. The relation between the remaining battery capacity against the storage time with the self-discharge resistance shows that this resistance value increase with the SOC until certain value as peak and then decreases with the time. The discharge resistance changes with the terminal voltage from the battery EMF especially during transient interval, and hence, depends on the discharge current. A rate of charge or discharge in Amperes is proportional to the capacity of the battery. As the state of charge increases, the internal resistance tends to decrease. Hence, the current increases leading to further increase of the state of charge accompanied by an increase in temperature. The linear assumption is usually not true. The nonlinearity is more evident for faster discharge rates. A better solution is to consider the manufacturer discharge curves and only use a linear approximation to interpolate the appropriate discharge curve.

4. Conclusion

In this paper, a review of different types of storage devices is presented with a focus on the modeling of Lead-Acid batteries that are the preferred choice as

storage unit in many applications especially for green energy. A flexible and efficient modeling method is proposed and validated with a 12 V, 4 Ah Lead-Acid battery. The parameters of the battery model were derived as functions of the state of charge (SOC) of the battery using curve fitting techniques and compared with the NP4-12 YUASA battery manufacturer's data sheet for different capacity rates. The discharge and charge characteristics of the battery model were studied and simulation results showed excellent matching. Furthermore, a neural network based learning system method with back-propagation techniques was implanted for parameters estimation using MATLAB which can readily be used to identify parameters and characteristics for this type of batteries with capacity ranging from 0.05 to 3 CA. It was shown that the neural models have the ability to predict values and also make interpolation between learning curves' data at various operating conditions. Finally, closed form nonlinear equations linking inputs and outputs without the need to train the neural network were presented and validated. The results indicated that the proposed model closely matched the actual data of the Lead-Acid battery verified using NP4-12 YUASA battery data sheet.

5. References

[1] John B., Aiming Z., Bo S., Kristen H., "Evaluating the potential of small scale renewable energy options to meet rural livelihoods: A GIS and life-cycle cost-based assessment of western china's options", Elsevier energy policy, 35. 2007, pp. 4391-4401.

[2] IEA, "Lead-Acid battery guide for stand-alone photovoltaic systems", IEA Task III, Report IEA-PVPS3-06 1999.

[3] Derek P., Frank C.W., "Industrial Electrochemistry" 2nd edition, Chapman and Hall, New York, 1990.

[4] Markus R., Hans-Peter B., Schneidegger R., "Minimizing the environmental impact of large-scale rural PV", Renewable energy world, James and James (science publishers) Ltd London, vol. 4, no. 1, 2001, pp. 47-59.

[5] Sathiakumar S. "An Investigation on the suitable battery system for marine Applications", School of Electrical and Information engineering, University of Sydney. Sydney, 2006.

[6] Reid C.E, "Chemical Thermodynamics", McGraw Hill Series in Advanced Chemistry. McGraw Hill Singapore, 1990.

[7] Sorensen B. "Renewable energy. Its physics, engineering, use, environmental impacts, economy, and planning aspects", 3rd edition. Elsevier science, Amsterdam, 2004.

[8] Yuasa Battery-Europe. Endurance Battery Manual, 1998.

[9] Battery characteristics: Teaching and Learning Packages. Department of Materials Science and Metallurgy, University of Cambridge. Dissemination of IT for the Promotion of Materials Science; http://www.doitpoms.ac.uk/tlplib/batteries/index.php

[10] Power-sonic Corporation, "Sealed Lead-Acid Batteries", Technical Handbook, 2008.

[11] Panasonic Ltd, "Overview of Lithium-Ion Batteries", Technical Manual, 2007.

[12] Sadli, I.; Marie-Joseph, I.; Primerose, A.; Clergeot, H., "New battery dynamic model: Application to lead-acid battery", The 2nd International Conference on Computer and Automation Engineering (ICCAE), 26-28 Feb. 2010, Vol. 5, pp. 140 – 145.

[13] Hartmann, L.V.; Correa, M.; Lima, A.M.N., Leao, J.F.A., "Lead-Acid battery modeling and state of charge monitoring", Applied Power Electronics Conference and Exposition (APEC), 2010 Twenty-Fifth Annual IEEE, 21-25 Feb. 2010, pp. 239 – 243.

[14] Bambang Sri Kaloko, Soebagio, Mauridhi Hery Purnomo, "Estimation of Residual Capacity of Lead Acid Battery using RBF Model," IJCA Special Issue on Artificial Intelligence Techniques - Novel Approaches & Practical Applications (3):12–17, 2011. Published by Foundation of Computer Science.

[15] Ganesan, A., Sundaram, S., "A Heuristic Algorithm for Determining State of Charge of a Lead Acid Battery for Small Engine Applications," SAE Technical Paper 2012-32-0082, 2012.

[16] Le, D. and Sisk, B., "Lead-Acid State of Charge Estimation for Start-Stop Applications," SAE Technical Paper 2013-01-1532, 2013.

[17] Ceraolo, M., "New dynamical models of Lead-Acid batteries", IEEE Transactions on Power Systems, Vol. 15, Issue 4, Nov. 2000, pp. 1184-1190.

[18] Salameh Z. M., Casacca M. A., and Lynch W. A., "A mathematical model for Lead-Acid batteries", IEEE Transactions on Energy Conversion, Vol. 7, No. 1, 1992, pp. 93-98.

[19] Matthias Dürr, Andrew Crudena, Sinclair Gaira and J. R. McDonalda, "Dynamic model of a Lead Acid battery for use in a domestic fuel cell system", Journal of Power Sources, Vol. 161, Issue 2, October 2006, pp. 1400-1411.

[20] Jantharamin N., Zhang, L.,"A new dynamic model for Lead-Acid batteries", 4th IET Conference on Power Electronics, Machines and Drives, April 2008, pp. 86-90.

[21] Chan H.L., Sutanto D., "A new battery model for use with battery energy storage systems and electric vehicles power systems", IEEE Power Engineering Society Winter Meeting, Vol. 1, pp. 470-475, 2000.

[22] NP valve regulated Lead Acid battery manual, Yuasa Battery Sale (UK) Ltd., 1991

[23] Adel El Shahat, "PM Synchronous Machine New Aspects; Modeling, control, and design", ISBN 978-3-659-25359-1, LAP Lambert Academic Publishing, Germany, 2012.

[24] Adel El Shahat, “DC-DC Converter Duty Cycle ANN Estimation for DG Applications”, Journal of Electrical Systems (JES), ISSN 1112-5209; Vol. 9, Issue 1, March 2013.
[25] Adel El Shahat, and Hamed El Shewy, “High Fundamental Frequency PM Synchronous Motor Design Neural Regression Function”, Journal of Electrical Engineering, ISSN 1582-4594; Article 10.1.14, Edition 1, March, Vol. 10, 2010.
[26] A. El Shahat, and H. El Shewy, “PM Synchronous Motor Control Strategies with Their Neural Network Regression Functions”, Journal of Electrical Systems (JES), ISSN 1112-5209; Vol. 5, Issue 4, Dec. 2009.
[27] Adel El Shahat, “Photovoltaic Power System Simulation for Micro – Grid Distribution Generation”, 8th International Conference on Electrical Engineering, 29-31 May, 2012, Military Technical College, Egypt; EE137, ICEENG 2012.
[28] A. El Shahat, H. El Shewy, “Neural Unit for PM Synchronous Machine Performance Improvement used for Renewable Energy”, Paper Ref.: 910, Global Conference on Renewable and Energy Efficiency for Desert Regions (GCREEDER2009), Amman, Jordan.
[29] S. Guo, S. Hillmansen, Y. Yin, J. Wang, “State of Health Monitoring of Lead-acid Batteries”, Proceedings of the 14th International Conference on Automation & Computing, pp. 250-254, Brunel University, West London, UK, 6 Sep. 2008.
[30] S. Guo, S. Hillmansen, J. Wang, “Model Based Analysis of Battery State of Health using Genetic Algorithms”, International Conference on Systems Engineering (ICSE), Coventry, 8-10 Sep. 2009.
[31] Mastragostino M., Soavi F., “Strategies for high-performance supercapacitors for HEV,” Journal of Power Sources 174, 2007, PP. 89–93.
[32] Halderman, James D - Martin, Tony - Batenburg, Craig Van, “Hybrid & Alternative Fuel Vehicles”, Prentice Hal, January 1, 2006
[33] Dhameja, S., “Electric vehicle battery systems”, Boston: Newnes, 2002.
[34] Falcon C.B. “Temperature Termination and the Thermal Characteristics of NiCd and NiMH Batteries”, In: WESCON/94. 'Idea/Microelectronics'. Conference Record, pp.309-315, 27-29 Sep 1994
[35] Adriana TRAISTARU, Ioan SORA, “Studies Concerning Li-ion Battery Thermal Behaviour in Low Temperature Environment”, Journal of Electrical Engineering: Volume 10 / 2010 - Edition: 1, pp. 135 – 140.
[36] Kuldeep Sahay, Bharti Dwivedi, “Supercapacitors Energy Storage Based DSTATCOM”, Journal of Electrical Engineering: Volume 10 / 2010 - Edition: 3, pp. 98 105
[37] Ashish saini, “Technical Overview of Different Energy Storage Technologies with Renewable Source”, Journal of Electrical Engineering: Volume 12 / 2012 - Edition: 2, pp. 201 208.
[38] Pawan Sharma, “Application of Ultracapacitors in an Electric Toy Vehicle”, Journal of Electrical Engineering: Volume 9 / 2009 - Edition: 2, pp. 101 107
[39] Andreas Steimel, “High-Power Hybrid Shunt Compensator with Superconducting Magnetic Energy”, Journal of Electrical Engineering: Volume 6 / 2006 - Edition: 3, pp. 12- 17
[40] Hirofumi Akagi, “Active Filters and Energy Storage Systems for Power Conditioning in Japan”, Journal of Electrical Engineering: Volume 6 / 2006 - Edition: 3, pp. 26 – 35
[41] Mohamed B. Zahran, Ali M. Yousef, “Photovoltaic Wind-Turbine Battery Hybrid System Monitoring”, Journal of Electrical Engineering: Volume 14 / 2014 - Edition: 1, pp. 376 – 386.
[42] G.Srinivasa Rao, G.Keseva Rao, S.Siva Naga Raju, “Automated Integrated Solar/Wind based Battery Charging System for Supercapacitor Stack used in Hybrid Electric Vehicle”, Journal of Electrical Engineering: Volume 14 / 2014 - Edition: 2, pp. 261-267.